Adaptive Thermal Boundary Conditions for Smoothed Particle Hydrodynamics

Kirk Fraser[1,2], Laszlo I. Kiss[1], Lyne St-George[1]
[1] *University of Quebec at Chicoutimi*
[2] *Predictive Engineering, Quebec Canada*

Abstract

Smoothed Particle Hydrodynamics (SPH) is a robust meshfree approach for the simulation of large plastic deformation processes such as high speed cutting, forging, extrusion, and friction welding. Often, heat transfer is an important consideration for such industrial processes; for this reason, the effects of heat loss from convection, radiation, or flux from the free surface should be included. However, because of the meshfree nature of SPH, the elements located at the free surface can change, and are not typically known at each time step. This difficulty makes application of thermal boundary conditions problematic in SPH simulations.

In this work, we describe a robust and efficient adaptive thermal boundary condition algorithm. Our approach uses a straightforward free surface extraction algorithm. Once the free surface elements are found, the appropriate thermal boundary condition can be applied. We describe the SPH boundary formulation for the Dirichlet (defined temperature), Neumann (defined flux), and Robin (convection) boundary conditions. The algorithm is validated against the finite element method and an example of an industrial application, friction stir welding, is presented.

Key-words

Smoothed Particle Hydrodynamics, Adaptive Thermal Boundary Conditions, Large Plastic Deformation, Computational Solid Mechanics, Friction Stir Welding, LS-DYNA® Users Conference 2016

Introduction

Numerical simulation of large deformation industrial processes such as forging, extrusion, high speed cutting, and friction stir welding has typically been a difficult task with mesh based methods. These processes, also known as solid state methods tend to lead to large levels of mesh distortion requiring the use of complicated and time consuming re-meshing algorithms. In recent years, a lot of work has gone into simulating these solid state processes with meshfree methods such as smooth particle hydrodynamics (SPH). In the SPH approach, the conservation equations are solved at particle points using a collocation type approach that does not require a background mesh. This differs from so called meshfree methods such as element free Galerkin (EFG) [1-5], finite point method (FPM) [6], and particle finite element method (PFEM) [7] among others that require a background mesh for numerical integration. SPH was originally developed by Lucy [8] and Gingold and Monaghan [9] in 1977 for astrophysics simulations. Since then, SPH has been applied to many different types of problems such as free surface fluid flows [10-14], magneto-hydrodynamics [15], casting [16-18], forging, [19], explosion welding [20], and high speed cutting [21, 22] to name a few.

A number of research groups have worked on simulating the friction stir welding process (FSW) with SPH. One of the first implementation was by Bhojwani [23] using an isothermal approach (in LS-DYNA). At that time, the code did not include heat transfer, thus, the important aspects of thermal softening could not be included. Since then, Timesli *et al.* [24], as well as Tartakovsky *et al.* [25], have developed a 2D SPH code to simulate FSW. Since their codes are 2D, their approach is best suited for thin plate welding or for the plunge phase where the thermal and stress gradients are negligible in the third dimension. Pan *et al.* [26] have worked on simulating the FSW process in 3D. They have focused on using a coupled thermal-fluid approach with a Sellars-Tegart material model. Their tactic does not allow them to determine defects, residual stresses, or distortions since elastic strains are not included in the fluid model. Fraser *et al.* [27, 28] have also focused on 3D simulation of FSW, however, they use a solid mechanics approach and are able to incorporate the effect of elastic strains. Both these research groups have included the important effects of thermal softening and solve for the temperature distribution in the work pieces using an SPH heat transfer algorithm.

In this paper, we will describe the implementation of an adaptive thermal boundary condition algorithm for SPH. Because of the meshfree nature of SPH, the free surface particles are not inherently known at each time step. We introduce a fast and efficient free surface detection algorithm along with the description of the formulation of the fixed temperature, flux, and convection SPH formulation. The algorithms are validated for a simple semi-infinite solid case. Following that, a cooling simulation of a friction stir welded joint is presented. The goal of the simulation is the prediction of the temperature distribution during cooling and the residual stresses.

The SPH Method for Heat Transfer

Conduction in a continuum is governed by the second order partial differential equation that is commonly referred to as the heat diffusion equation. In its most general form, the equation is:

$$\rho C_p \frac{\partial T}{\partial t} = \nabla \cdot (k \nabla T) + \dot{q} \qquad \textbf{Eqn 1}$$

Here we have made no assumptions as to the dependence of the thermal conductivity, k, on temperature or space. ρ is the density of the material, $C_p$is the specific heat capacity, T is the temperature, t is the time, $\dot{q}$ is a heat generation heat (W/m^3), and ∇ is the nabla operator.

In solving the parabolic PDE, we must discretize the domain into material points. Because of this discretization, we can safely presume that k is at most a function of temperature (if k is a function of position, it can be given a different value at the discretization points). This allows the thermal conductivity to be moved outside of the influence of the gradient operator:

$$\frac{\partial T}{\partial t} = \frac{1}{\rho C_p}(k\nabla^2 T + \dot{q}) \qquad \textbf{Eqn 2}$$

With this form of the heat equation in mind, we must then find an SPH approximation for the Laplace operator (∇^2). According to Jubelgas [29], an appropriate SPH approximation of the Laplace operator is:

$$\nabla^2 F = 2\sum_{j=1}^{N_i} \frac{m_j}{\rho_j} \frac{(T_i - T_j)}{|x_{ij}|^2} x_{ij} \frac{\partial W_{ij}}{\partial x_i{}^\beta} \qquad \textbf{Eqn 3}$$

where m_j/ρ_j is the volume of the j^{th} particle, T_i and T_j are the temperature at the i^{th} and j^{th} particles, N_i is the number of neighbors of the i^{th} particle, $x_{ij} = x_i - x_j$ is the position vector between the two particles, and $\partial W_{ij}/\partial x_i{}^\beta$ is the gradient of the smoothing function (for the sake of brevity, the details are not provided here, the interested reader should consult [15, 30-33] among others). Applying the SPH approximation of ∇^2 to the heat conduction equation leads to:

$$\frac{dT_i}{dt} = \frac{1}{\rho_i C_{p_i}} \sum_{j=1}^{N_i} \frac{m_j}{\rho_j} \frac{(k_i + k_j)(T_i - T_j)}{|x_{ij}|^2} x_{ij} \frac{\partial W_{ij}}{\partial x_i{}^\beta} \qquad \textbf{Eqn 4}$$

This formulation gives very good results as long as the difference between k_i and k_j is not significant (spatial variation of k due to temperature dependence. However, when k is a function of temperature ($k(T)$), **Error! Reference source not found.** is not precise and should be written as:

$$\frac{\partial T}{\partial t} = \frac{1}{\rho C_p}\left(k\nabla^2 T + \frac{dk}{dT}(\nabla \mathrm{T})^2 + \dot{q}\right) \qquad \textbf{Eqn 5}$$

Eqn 5 uses the expansion of $\nabla \cdot (k\nabla T)$ by the product rule. The $dk/dT\,(\nabla \mathrm{T})^2$ term can be reasonably approximated by using the harmonic mean for the thermal conductivity (Cleary and Monaghan [34])instead of the arithmetic mean, the SPH heat diffusion equation takes the form:

$$\frac{dT_i}{dt} = \frac{1}{\rho_i C_{p_i}} \sum_{j=1}^{N_i} \frac{m_j}{\rho_j} \frac{(4k_i k_j)}{(k_i + k_j)} \frac{(T_i - T_j)}{|x_{ij}|^2} x_{ij} \frac{\partial W_{ij}}{\partial x_i{}^\beta} \qquad \textbf{Eqn 6}$$

This formulation has been shown to give good results for ordered and disordered particles. The variation in the thermal conductivity can be greater than a factor of ten with this approach. This is the formulation that is used in SPHriction-3D. The heat diffusion equation is integrated in time using a forward difference scheme (explicit). Rook *et al.* [35] have developed an implicit heat transfer algorithm for SPH. However, for most solid state industrial processes, a coupled thermal-mechanical solution is used and the time step is governed by the speed of sound in the material. For this reason there is no advantage to using an implicit HT solution approach.

Surface Detection and Normal Vectors

Before treating SPH thermal boundary conditions, we need to have a methodology to determine the particle on the free surface of the SPH domain. This is very important for setting up a general tactic to describe surface heat flux and convection.

In order to determine the particle surface normal, we can use the fact that particles on the surface of the SPH domain have an incomplete set of neighbors. We can find a vector (${x_{COM}}_i^{\alpha}$) between the i^{th} particle and the center of the particle cluster by:

$${x_{COM}}_i^{\alpha} = \frac{1}{M}\sum_{j=1}^{N_i} m_j {x_{ij}}^{\alpha} \qquad \textbf{Eqn 7}$$

This can be thought of as a normal vector pointing out of the solid at each surface particle. The total mass of the particle cluster is M, the mass of the j^{th} particle is m_j, and the distance vector between the i^{th} and the j^{th} particle is x_{ij}. We immediately recognize that the particles that are within the body of the solid will essentially have a null value for ${x_{COM}}_i^{\alpha}$. Next, we need to be able to evaluate which particles reside on the surface of the solid domain. This can be accomplished by comparing the length of the normal vector to the smoothing length, h_i, of the particle and to a problem specific number of neighbors, ξ.

$$Surface_{node} = \begin{cases} 1, & x_{COM_i} \geq \frac{1}{4} h_i \; and \; N_i \leq \xi \\ 0, & Otherwise \end{cases} \qquad \textbf{Eqn 8}$$

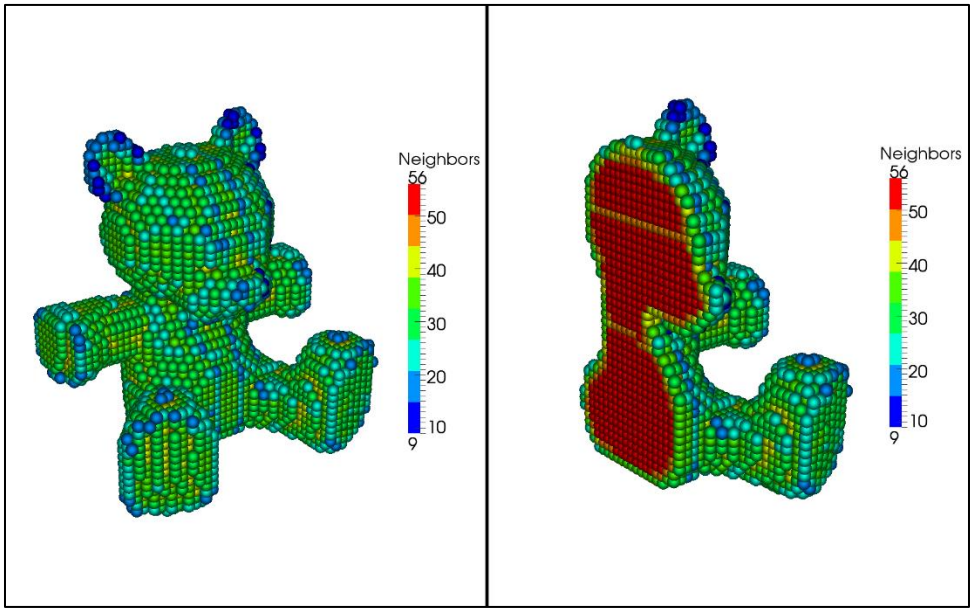

Figure 1 – SPH neighbors for the solid body

In this manner, the particles that are on the surface of the domain will be tagged with a value of one and the internal particles will be tagged with a value of zero. We have typically been using $\xi \approx 44$ in 3D with the smoothing length factor of 1.2; however, the number of neighbors used as the cutoff is problem specific. A general procedure is to run the model without the surface and normal extraction and investigate the neighbors. Figure 1 shows the neighbors for a general solid body; we can see that the particles on the surface of the body generally have less than ~44 neighbors. The surface normal vectors

are important for the thermal boundary conditions (in order to determine the surface particles) as well as for the contact algorithm (not discussed in this paper, see Fraser *et al.* [21] for full details).

We can see how well the algorithm works for an arbitrary shaped domain (a solid teddy bear) in Figure 2. The left side of the image shows the normal vectors and the right side shows only the surface particles.

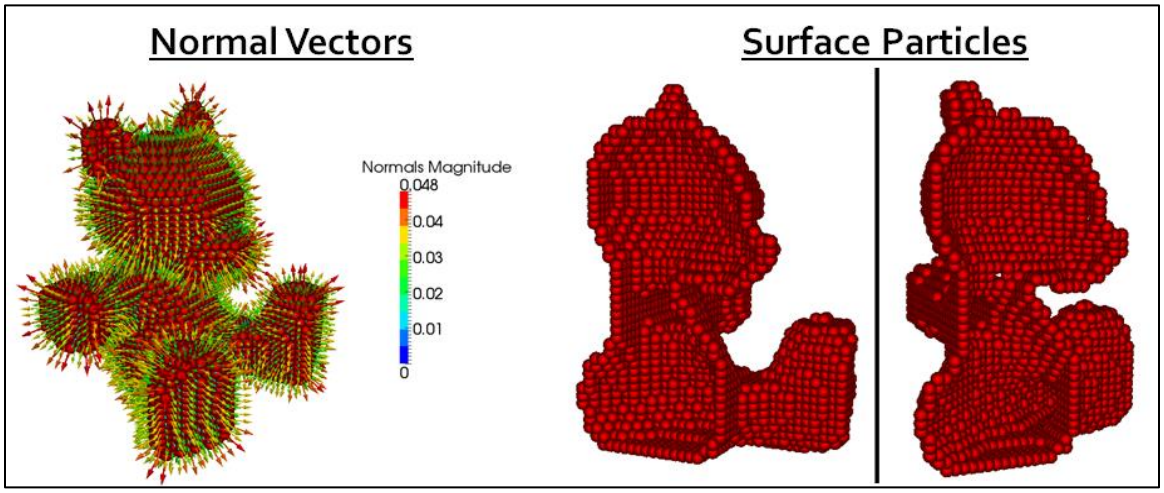

Figure 2 – Normal vectors and surface particles

We are not the first to come up with a normal vector and surface extraction algorithm. To our knowledge, we are one of the only groups to evaluate the normal vectors using the center of mass concept. Marrone *et al.* [36] use an algorithm that is ideal for fluid simulations. They use a two-step method, first the particles that are close to the free surface are found by using the properties from the renormalization matrix. Then in the second step, they evaluate the geometric properties of the SPH elements found in the first step. Their process requires scanning a conical region beyond the surface elements. Their method supposes that the renormalization approach has been used. Our method is much less complicated as we simply need to find the center of mass. This is accomplished with a very simple equation that is evaluated very quickly. Other authors such as Randles and Libersky [37] have used a "discrete color" approach. The color of the particles is evaluated by exploiting the completeness of the interpolation of a SPH element. If the interpolation is incomplete, the element is assigned a color that associates it as a boundary particle.

Thermal Boundary Conditions

The particular solution of an ODE or a PDE requires boundary conditions and/or initial conditions. In this sub-section, we will discuss how the three main thermal BCs are implemented in SPHriciton-3D:

1. Imposed surface temperature – this is a Dirichlet type boundary condition (1st type), the value of the function is specified on the boundary for the duration of the simulation
2. Imposed heat flux – this is a Neumann type boundary condition (2nd type), the value of the gradient of the function is specified on the boundary
3. Surface convection – this is a Robin type boundary condition (3rd type), a linear combination of the value of the function and is derivative are provided

A schematic of the four main boundary conditions is provided in Figure 3. The mathematic definition of the boundary condition as well as a representation of the condition is given in the image.

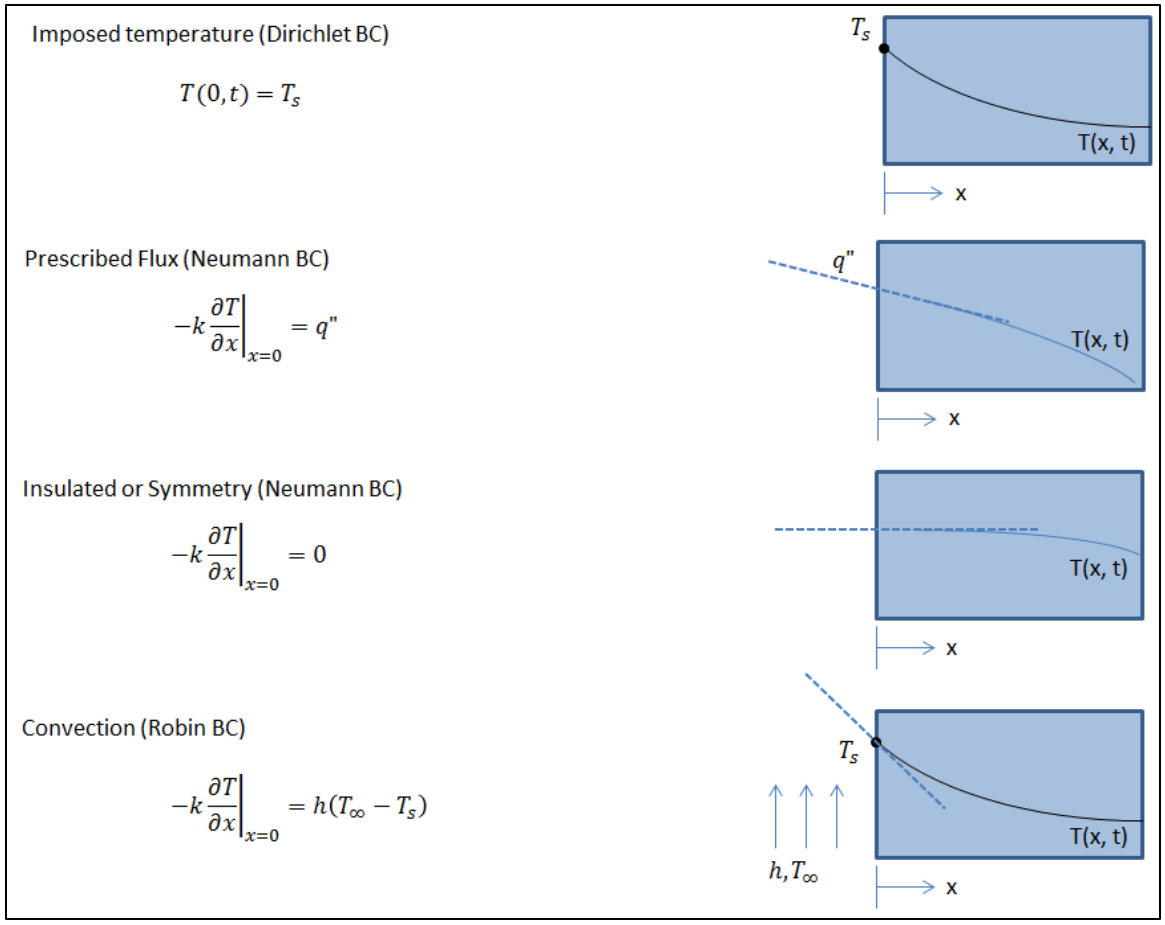

Figure 3 – Thermal boundary conditions

Isothermal Surface

The isothermal boundary condition can easily be enforced by constraining the nodal temperature of the concerned SPH elements. A value for the temperature can be prescribed at the beginning of the simulation. The prescribed temperature can be a function of time if needed. It is important to exclude the SPH elements with a prescribed temperature from the temporal integration. Using this approach the Dirichlet BC can be enforced exactly in SPH.

Isothermal BC Validation

We can use the semi-infinite solid approximation as a validation against the results from SPHriction-3D. Figure 4 shows the solid block with the initial temperature field and the final temperature after 200.0 seconds. The whole block is initially at 20°C except for the end that is held at 500°C.

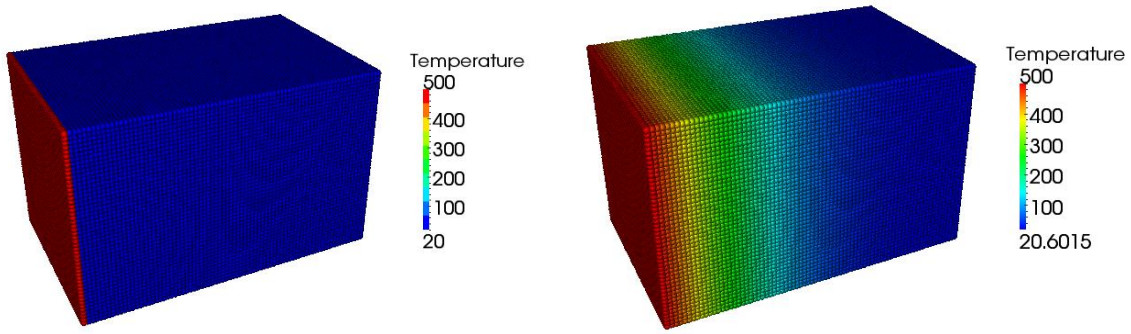

Figure 4 – Initial and final temperature field (t = 200.0 s)

The temperature of the block as a function of time and space can be found from:

$$T(x,t) = T_s + (T_i - T_s)\text{erf}\left(\frac{x}{2\sqrt{\alpha t}}\right) \qquad \textbf{Eqn 9}$$

Where T is the temperature at a point for a specific time, t. T_s is the isothermal end temperature, T_i is the initial temperature of the block, erf is the Gaussian error function, x is the axial location along the block, and α is a material specific thermal constant. The results for the first 50 seconds of the simulation are shown in Figure 5.

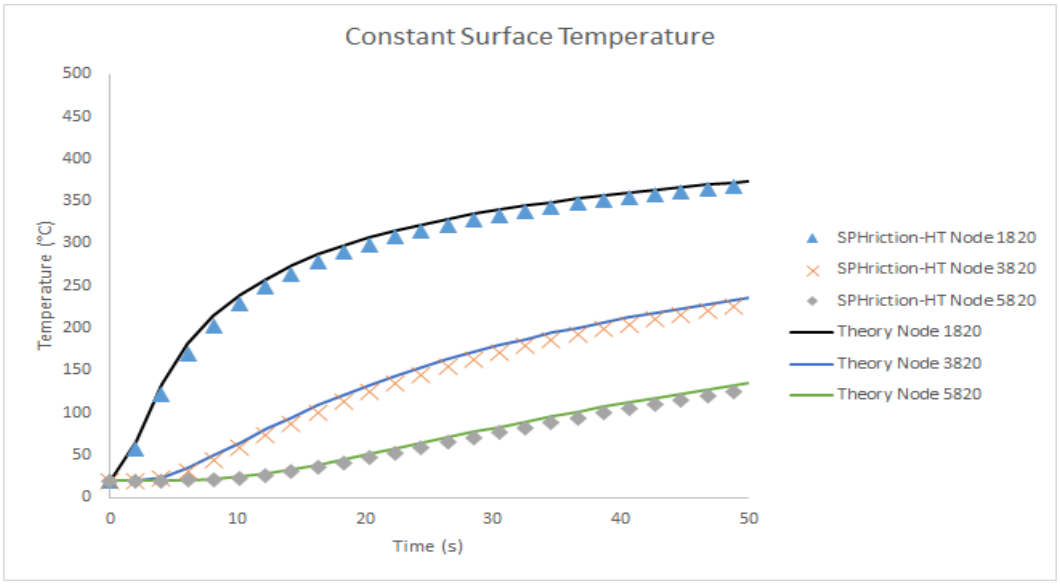

Figure 5 – Nodal temperatures (comparison between theory and SPHriction-3D)

Surface Heat Flux

The heat flux, q", boundary condition can be formulated by recognizing that heat is flowing through the surface of the solid body. The quantity of energy (q) flowing through the surface per unit of time will be:

$$q = q"A_s \qquad \textbf{Eqn 10}$$

where A_s is the area of the surface that heat is flowing through. Since we are working with a discretized solid body, we can recognize that the heat is flowing through individual surface segments that are associated to individual SPH elements. We can determine the temperature increase per unit time for a surface particle from:

$$\frac{dT_i}{dt} = \frac{q_i}{m_i C_{p_i}} = \frac{q"_i A_i}{m_i C_{p_i}} \qquad \textbf{Eqn 11}$$

where A_i is the associated surface area of an SPH element. Figure 6 shows a schematic of the surface area of an SPH element for a uniform grid. The surface area is the square of the inter particle distance.

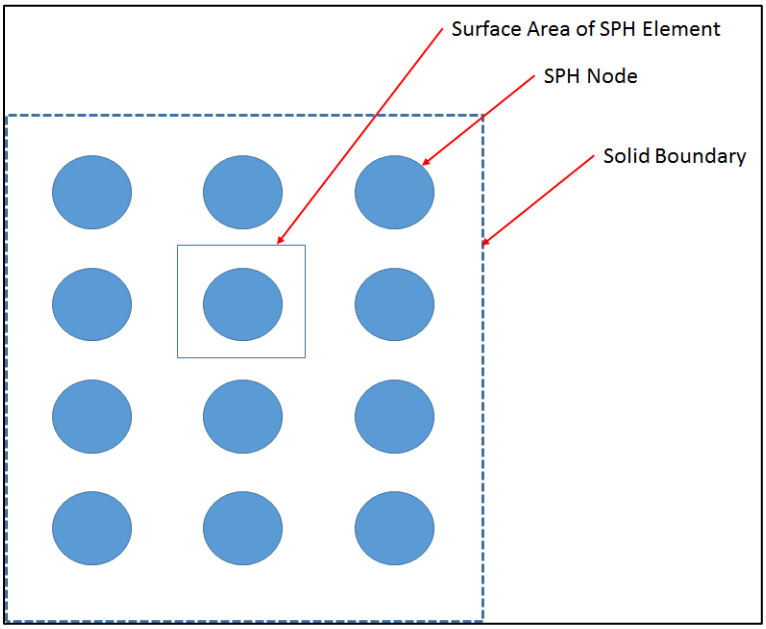

Figure 6 – Typical surface area for a uniform distribution

For a uniform distribution of SPH elements on the surface of the solid domain, the following SPH formulation gives excellent results:

$$\frac{dT_i}{dt} = \frac{1}{\rho_i C_{p_i}} \sum_{j=1}^{N_i} \frac{m_j}{\rho_j} \frac{(4k_i k_j)}{(k_i + k_j)} \frac{(T_i - T_j)}{|x_{ij}|^2} x_{ij} \frac{\partial W_{ij}}{\partial x_i^{\beta}} + \frac{q"_i A_i}{m_i C_{p_i}} \qquad \textbf{Eqn 12}$$

A simple evaluation of the units on the left and right hand side of the equation shows that the units balance as they should:

$$\frac{dT}{dt}\left[\frac{K}{S}\right] = \frac{q"_i A_i}{m_i C_{p_i}}\left[\frac{K}{S}\right]$$

On the other hand, for non-uniform particle distributions, the above approach may not give accurate results. The heat flux boundary condition can be written using an SPH approach such that:

$$\frac{dT_i}{dt} = \frac{1}{\rho_i C_{p_i}} \sum_{j=1}^{N_i} \frac{m_j}{\rho_j} \frac{(4k_i k_j)}{(k_i + k_j)} \frac{(T_i - T_j)}{|x_{ij}|^2} x_{ij} \frac{\partial W_{ij}}{\partial x_i^{\beta}} + \frac{1}{m_i C_{p_i}} \sum_{j \in surface} \frac{m_j}{\rho_j} q"_j A_j W_{ij_{2D}} \qquad \textbf{Eqn 13}$$

In this formulation, the SPH sum for the heat flux term is performed only on the surface nodes and $W_{ij_{2D}}$ is a 2D smoothing kernel that is consistent with the kernel used for the conduction part of the equation. In

order to use this formulation, a neighbor list that operates on the surface nodes only is needed. This can easily be accomplished because we have already determined which SPH elements reside on the surface.

Surface Flux Validation

The validation test model for the surface flux will be a semi-infinite solid. One end of the solid will be given a prescribed heat flux boundary condition. The model is created in LS-DYNA using finite elements and in SPHriction-3D using SPH elements. All the parameters are the same in both models. A surface heat flux of 1.0E+05 W/m^2 is specified on the left end of the block. Figure 7 shows the results from LS-DYNA and SPHriciton-3D. The magnitude and location of the temperature field is the same in both cases.

LS-DYNA **SPHriction-3D**

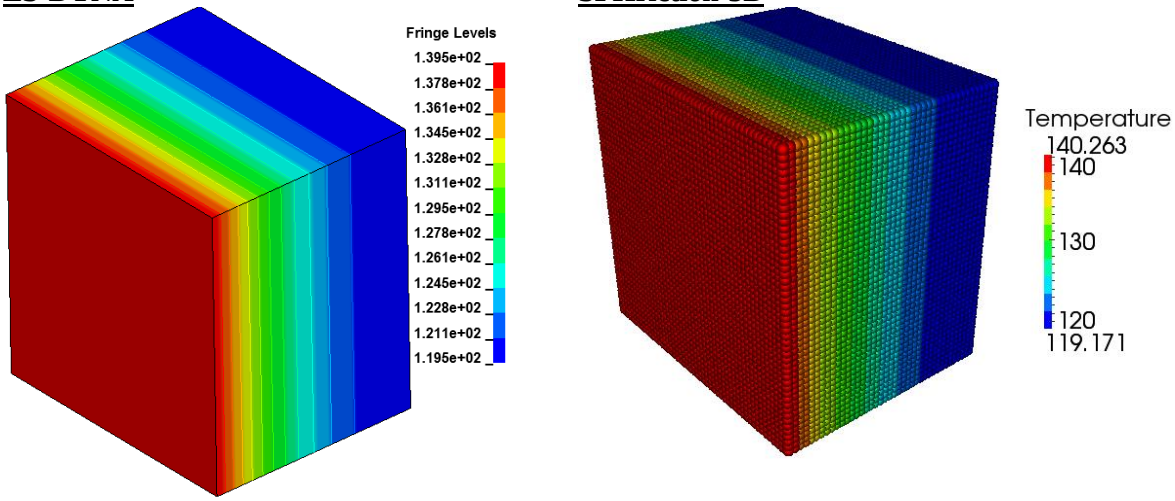

Figure 7 – End heat flux BC results comparison

The evolution of the temperature at three nodes is shown in Figure 8 for the LS-DYNA and SPHriction-3D results. The node locations are at x = 0, x = 1/2L and x = L. The SPHriction-3D solution tracks directly over the LS-DYNA solution.

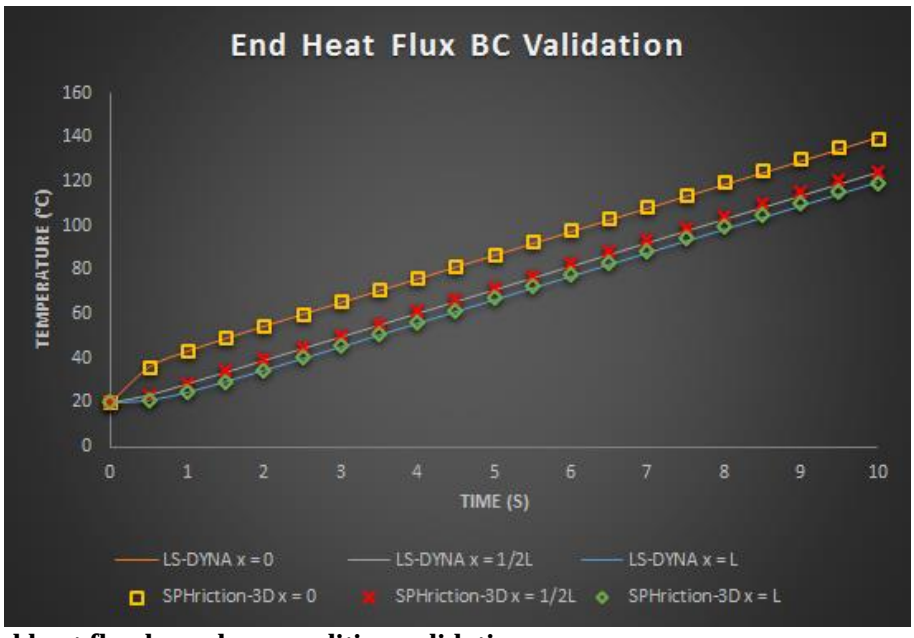

Figure 8 – End heat flux boundary condition validation

Surface Convection

Convective heat transfer from the surface of the aluminum work pieces is an important part of the puzzle. Without convection, the simulated temperature will be much higher than they should be. The development of the convection boundary condition follows very closely that of heat flux BC. The heat flux through the surface is replaced by:

$$q" = h_{conv}(T_\infty - T_s) \qquad \textbf{Eqn 14}$$

where h_{conv} is the coefficient of convection at the free surface, T_s is the surface temperature, and T_∞ is the free stream temperature. The surface temperature should be very close to the nodal temperature of a SPH element on the boundary. We can now write the SPH heat equation with convection boundary conditions for a uniform grid:

$$\frac{dT_i}{dt} = \frac{1}{\rho_i C_{p_i}} \sum_{j=1}^{N_i} \frac{m_j}{\rho_j} \frac{(4k_i k_j)}{(k_i + k_j)} \frac{(T_i - T_j)}{|x_{ij}|^2} x_{ij} \frac{\partial W_{ij}}{\partial x_i{}^\beta} + \frac{h_{conv_i} A_i (T_\infty - T_i)}{m_i C_{p_i}} \qquad \textbf{Eqn 15}$$

As with the heat flux BC, A_i is the surface area of an SPH element on the solid boundary. The equation can also be used to approximate radiation boundary conditions since the coefficient of convection can easily be a function of temperature in the code. For a non-uniform particle spacing, the following is expected to give a better approximation:

$$\frac{dT_i}{dt} = \frac{1}{\rho_i C_{p_i}} \sum_{j=1}^{N_i} \frac{m_j}{\rho_j} \frac{(4k_i k_j)}{(k_i + k_j)} \frac{(T_i - T_j)}{|x_{ij}|^2} x_{ij} \frac{\partial W_{ij}}{\partial x_i{}^\beta} + \frac{1}{m_i C_{p_i}} \sum_{j \in surface} \frac{m_j}{\rho_j} h_{conv_j} A_j (T_\infty - T_j) W_{ij_{2D}} \qquad \textbf{Eqn 16}$$

We can again check the units:

$$\frac{dT}{dt}\left[\frac{K}{S}\right] = \frac{h_{conv_i} A_i (T_\infty - T_i)}{m_i C_{p_i}}\left[\frac{K}{S}\right]$$

Convection BC Validation

A simulation model is built in LS-DYNA with Finite elements and in SPHriction-3D with SPH elements in order to validate the convection boundary condition. In the first case, the block is initially at 20°C, and the left end is heated with a convection boundary condition. The same parameters are used in both models. The coefficient of convection is set to 100.0 W/m^{2}K and the external temperature is set at 500°C. The specific heat capacity and thermal conductivity of the solid are set to 1.0 J/kgK and 3000.0 W/mK. The simulation runs for 10.0 seconds. A graphical results comparison is provided in Figure 9. We can see that the temperature contours and the relative magnitude of the temperature is essentially the same in LS-DYNA and SPHriction-3D.

LS-DYNA **SPHriction-3D**

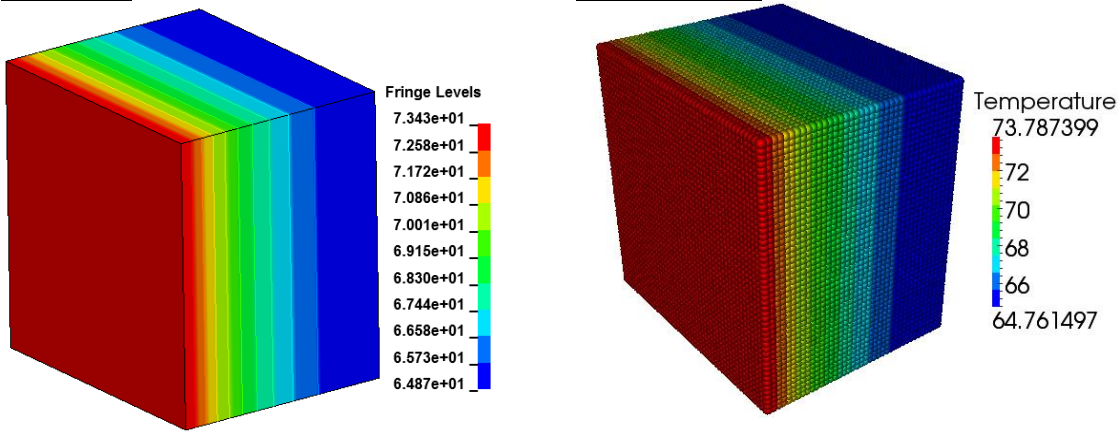

Figure 9 – Convection BC on one surface of block

Let's take a closer look at how the temperature varies at three discrete points in the solid throughout the simulation. We will investigate at x = 0, x = 1/2L and x = L. The results are shown in Figure 10, we can see that the values obtained from SPHriction-3D agree very well with the values obtained from LS-DYNA.

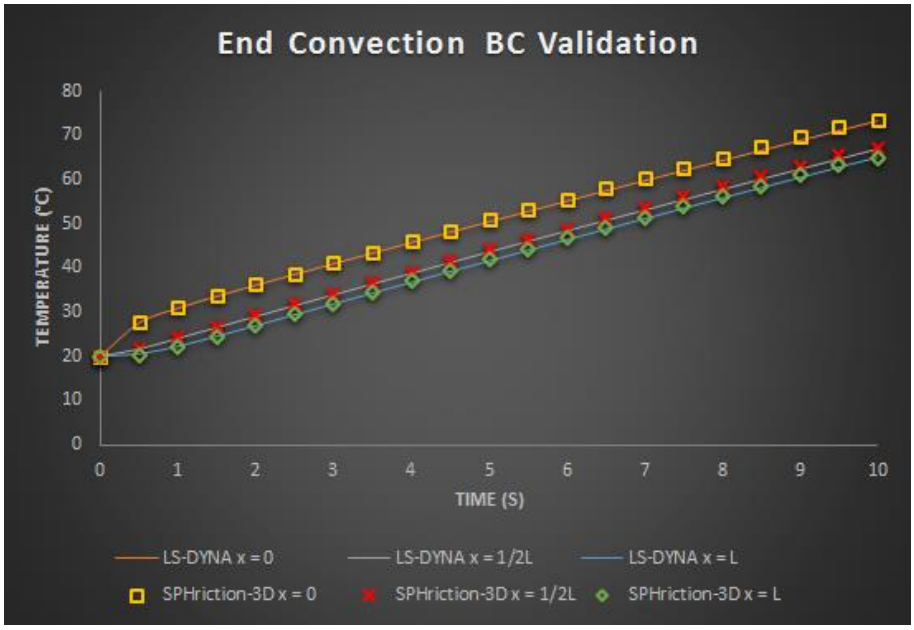

Figure 10 – Results comparison for end convection validation case

More often than not, the convection must be applied to all of the surfaces of the solid body. In Figure 11, the same convection conditions are applied to all the free surfaces of the model. Here, the results for the temperature distribution are shown at the end of the simulation (t = 10.0s). We can see that the temperature distribution is the same in LS-DYNA and SPHriction-3D. The magnitude of the temperature is not an exact fit because the SPH method suffers from incomplete interpolation; never the less, the results are very good.

LS-DYNA **SPHriction-3D**

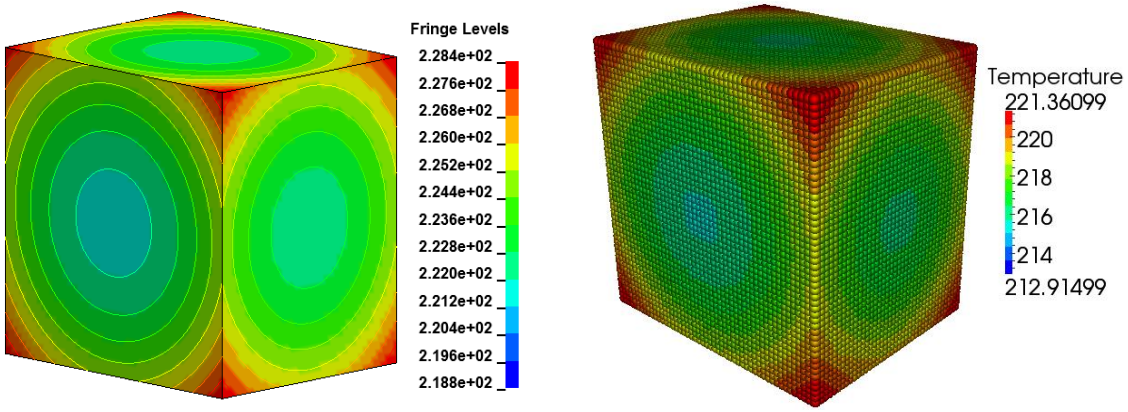

Figure 11 – All surface convection boundary condition

Industrial Example – Cooling of a FSW Joint

We are now in a position to use the new algorithm to determine the residual stresses in a friction stir welded joint. The new adaptive thermal boundary conditions will allow us to remove heat from the free surface of the work pieces and predict the final deformed shape and the locked in stresses. The friction stir welding process can be explained by the four main phases of the process:

Phase 1 – Plunge: The FSW tool is pressed into the work pieces (WPs) with a fixed rpm
Phase 2 – Dwell: The FSW tool remains stationary with a fixed rpm. This phase serves to continue to heat the WPs
Phase 3 – Advance: The FSW tool advances with a constant velocity and rpm. The weld is formed during this phase
Phase 4 – Cooling: The tool is retracted and the completed joint cools to room temperature

During Phase 1 and 3, enormous levels of plastic deformation occur in the aluminum in the region close to the tool (mechanically affected zone). These are the phases that are responsible for creating a high strength weld. As the WPs cool in Phase 4, the locked in stresses are redistributed. The final deformed shape of the plates and the residual stresses are found when the WPs have completely cooled.

Table 1 – Material properties used in cooling analysis

Parameter	6061-T6 (Work Piece)	Base and Tool (Steel)
k *(W/mK)*	175	55
ρ (kg/m^3)	2700	7850
C_p (J/kgK)	895	485
E (GPa)	70	200
σ_{y0} (MPa)	324	N/A
T_{melt} (°C)	580	N/A
T_{room} (°C)	20	N/A
m	1.34	N/A

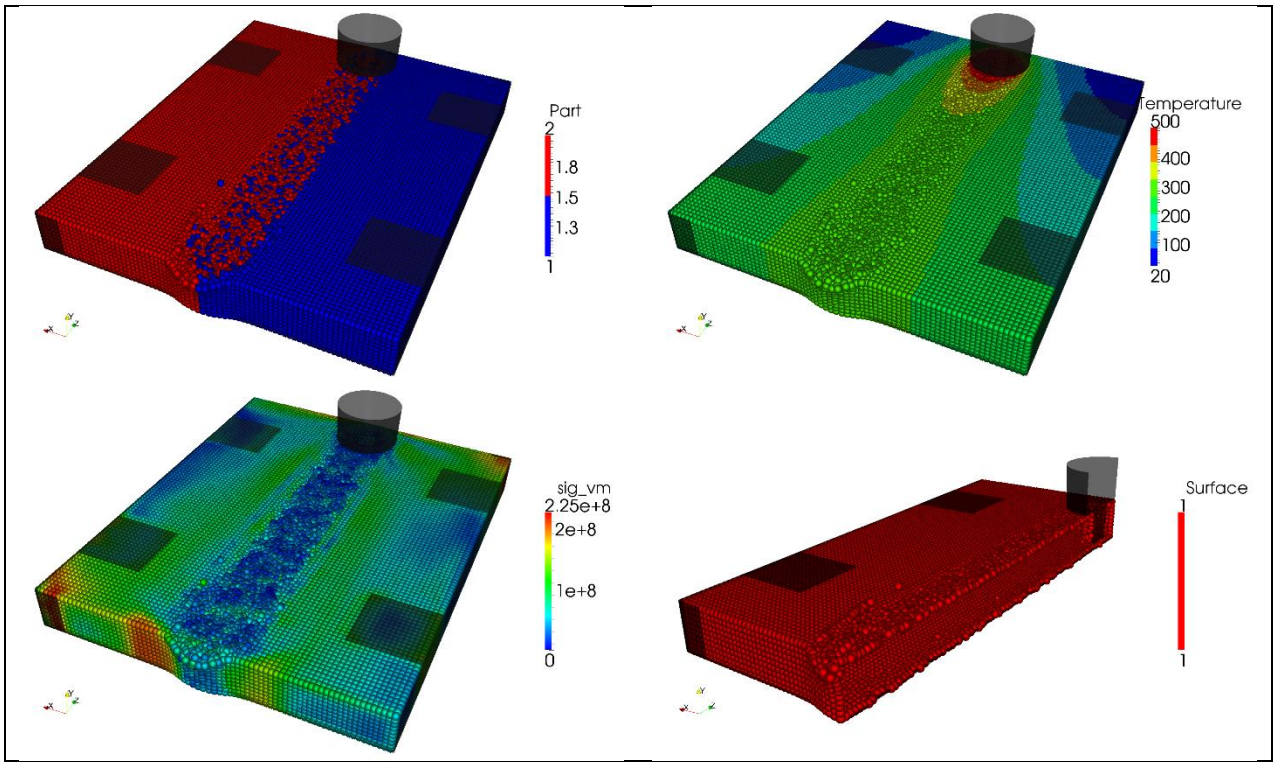

Figure 12 – Initial conditions at start of cooling analysis (clockwise from top left): Mixing results in the weld zone; temperature distribution (°C); effective stress (Pa), surface particles

A fully coupled thermal-mechanical approach is used based on Fraser et al. [21, 38]. The simulation starts from the final state of a FSW simulation (end of Phase 3) with 800 rpm and 660 mm/min advance. A video of all the phases of the FSW process (clamp, plunge, dwell, advance, retract, cool) can be viewed here: https://www.youtube.com/watch?v=pbjZnLV3yXA. The initial conditions for the cooling analysis are shown in Figure 12. The material properties are shown in Table 1. The convection coefficient, h_{conv} is taken as $10\,W/m^2K$. Time scaling is used for the cooling simulation since the time to cool the plate entirely is on the order of ~ 30 minutes. Since the mechanical deformation is very minimal during the cooling phase, we have found that we can use a time scaling factor of 1000 without incurring momentum errors (ratio of kinetic energy to internal energy remain small). To accomplish this, the thermal conductivity and the heat loss coefficient are scaled accordingly. A thermal softening perfect plasticity model is used for the aluminum work pieces of the form:

$$\sigma_y = \sigma_{y0}\left(1 - \left(\frac{T - T_{room}}{T_{melt} - T_{room}}\right)^m\right) \qquad \textbf{Eqn 17}$$

We have typically been painting the surface of the work pieces a mat black in order to capture the temperature distribution with an infrared camera (IRcam) during the FSW process. The emissivity of the paint, ε, is ~ 0.95. Because of this, we have found that heat loss due to radiation accounts for a large portion of the heat loss. The model that we have used for this simulation follows closely the development for convection. The total heat flux at the surface is then a combination of that from convection ($q"_{conv}$) and radiation ($q"_{rad}$):

$$q"_{total} = q"_{conv} + q"_{rad} = h_{conv}(T_\infty - T_s) + \varepsilon\sigma_{SB}({T_{surr}}^4 - {T_s}^4) \qquad \textbf{Eqn 18}$$

σ_{SB} is the Stefan Boltzmann constant ($5.67\text{x}10^{-8}$ W/m^{2}K^4) and T_{surr} is the temperature of the surroundings (taken as 20°C). Figure 13 shows the temperature distribution in the finished weld (using

the IRcam). We can see that the temperature distribution predicted by SPHriction-3D (see upper right image in Figure 12) is in good agreement with the IRcam image. Note that the temperature in the weld track cannot be measured by IRcam since this zone does not have the mat black paint. The emissivity of the aluminum in the unpainted weld zone is very low (~ 0.1) and leads to an inaccurate reading of the temperature.

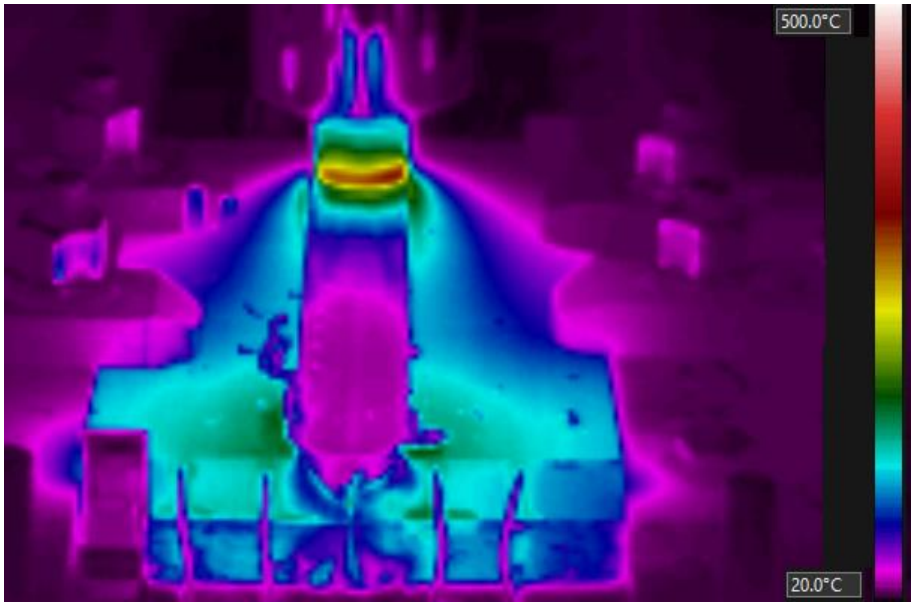

Figure 13 – IRcam image from FSW experiment at end of advancing phase

The temperature distributions for four different points in time are shown in Figure 14. We can see that the distributions are strongly influenced by the location of the supports and that the last region of the WPs to cool is the weld zone. This is because the supports are made of steel and have a significant thermal mass to absorb the energy from the WPs.

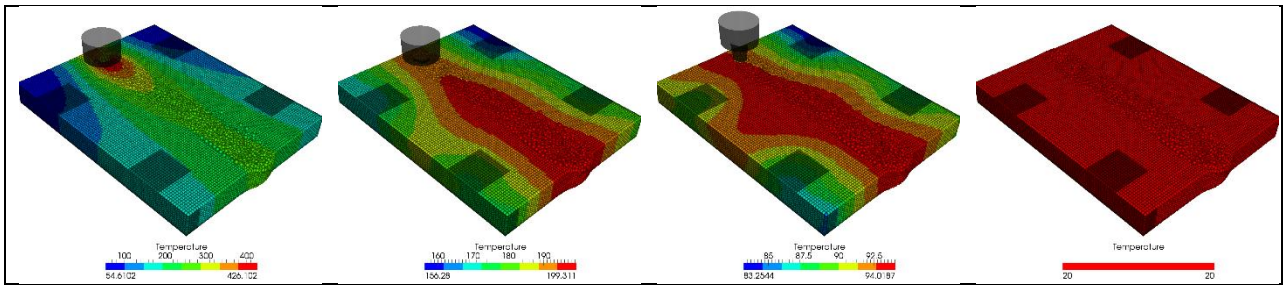

Figure 14 – Temperature profiles for (from left to right): t = 24 s, 32 s, 105 s, and 524 s (final step)

Four "thermocouples" were inserted into the WPs in order to record the temperature history throughout the simulation. The temperature at a so called "thermocouple" or TC for short is determined in the SPH simulation model by interpolating from a set of SPH points in the neighborhood of the TC. In this sense, the temperature at the i^{th} TC is:

$$T_{TC_i} = \frac{\sum_{j=1}^{N_i} \frac{m_j}{\rho_j} T_j W_{ij}}{\sum_{j=1}^{N_i} \frac{m_j}{\rho_j} W_{ij}} \qquad \textbf{Eqn 19}$$

TC3 and TC4 are inserted on the retreating and advancing side of the weld, 5mm from the weld line. TC1 and TC5 are 23 mm from the weld line (again on the retreating and advancing side). All thermocouples are embedded at a distance of one quarter the length of the WPs (from the end of the weld) and 2.5 mm deep from the surface of the WPs. Figure 15 shows the temperature history for the four TCs. From the graph, we are able to infer that the region closest to the weld zone are hottest. Furthermore, according to the simulation results, the temperature on the retreating side is slightly hotter than that on the advancing side. This can be explained by the movement of the material: as the tool rotates, the material on the advancing side is heated and transported to the retreating side.

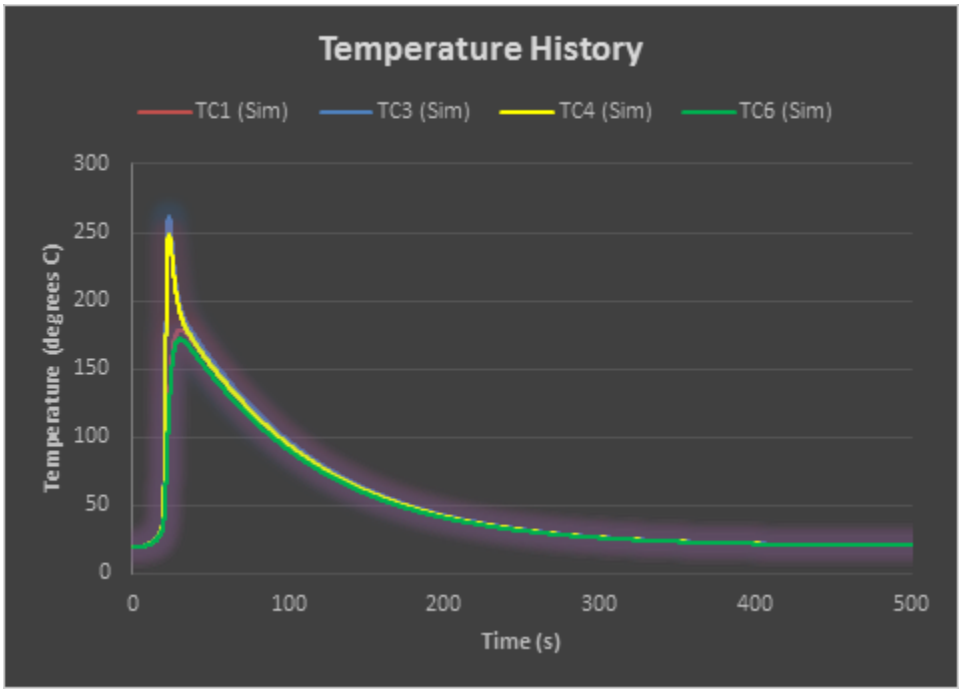

Figure 15 – Temperature history for TC1, TC3, TC4, and TC6

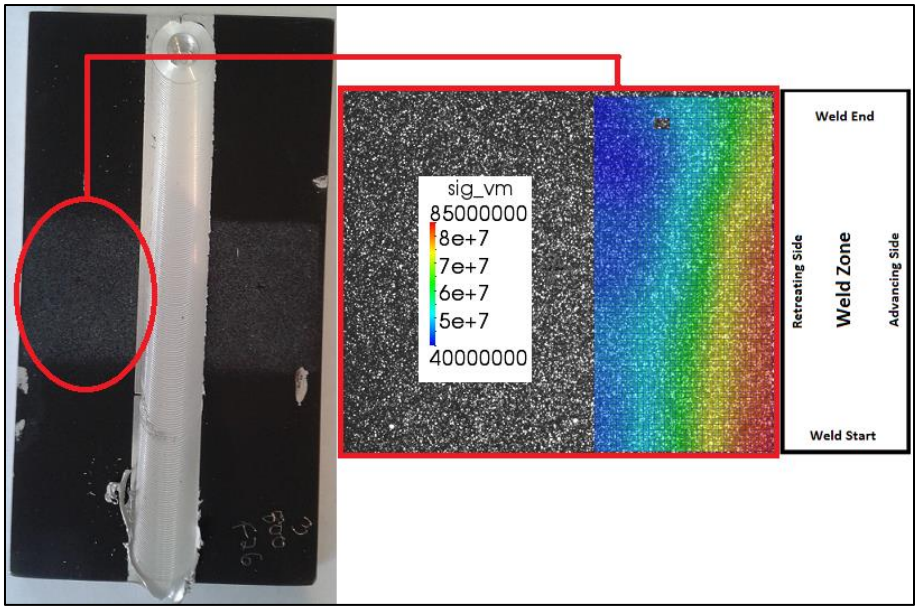

Figure 16 – Residual stress results from FSW experiment using DIC

We have used a Digital Image Correlation (DIC) (http://www.gom.com/metrology-systems/system-overview/aramis.html) system called ARAMIS, developed by GOM. The system is used to determine the residual stresses in the work pieces. A stochastic pattern was painted on the un-welded plates. The software is able to calculate the deformation on the surface of the plate by comparing the deformed state to the initial (reference) image. The measured residual stresses (showing effective stress in Pa) from experiment are shown in Figure 16. The residual stresses cannot be measured in the weld zone because of the large plastic deformation and mixing present in the weld track. The residual stresses determined at the end of the SPH simulation are shown in Figure 17. The highest stresses are concentrated close to the weld zone as was found experimentally.

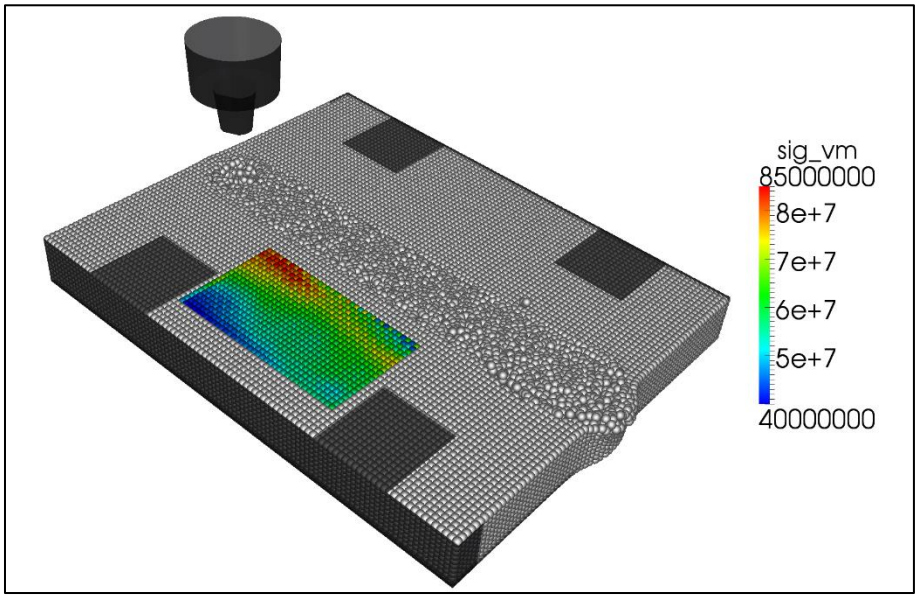

Figure 17 – Predicted residual stress from SPH model

The stress contours found experimentally and numerically are in close agreement. Differences are mainly due to the complex nature of the heat loss through from the WPs to the supporting structure. We can see in Figure 13 that the welded plates are much hotter than the supporting structure, once the weld is finished, heat flows into the steel supporting structure quickly cooling the WPs. Other discrepancies are explained by the difference in measuring techniques; the DIC method we have used provides a 2D approximation of the stresses on the surface, whereas the SPH model is full 3D.

Conclusion

In this work, we have described a robust and efficient adaptive thermal boundary condition algorithm that allows the accurate simulation of industrial processes where the mechanical behavior is strongly affected by the temperature history in the domain. We have shown that the algorithm gives good results in comparison to the finite element method for fixed temperature flux and convection boundary conditions. We have also shown an application of the proposed method for determining the residual stresses and distortions in a friction stir welding joint.

References

[1] Belytschko T, Fleming M. Smoothing, enrichment and contact in the element-free Galerkin method. Computers & Structures. 1999;71:173-95.
[2] Belytschko T, Lu YY, Gu L. Element-free Galerkin methods. International Journal for Numerical Methods in Engineering. 1994;37:229-56.

[3] Belytschko T, Organ D, Gerlach C. Element-free galerkin methods for dynamic fracture in concrete. Computer Methods in Applied Mechanics and Engineering. 2000;187:385-99.
[4] Krysl P, Belytschko T. Analysis of thin shells by the Element-Free Galerkin method. International Journal of Solids and Structures. 1996;33:3057-80.
[5] Krysl P, Belytschko T. Element-free Galerkin method: Convergence of the continuous and discontinuous shape functions. Computer Methods in Applied Mechanics and Engineering. 1997;148:257-77.
[6] Onate E, Idelsohn S, Zienkiewicz OC, Taylor RL. A FINITE POINT METHOD IN COMPUTATIONAL MECHANICS. APPLICATIONS TO CONVECTIVE TRANSPORT AND FLUID FLOW. International Journal for Numerical Methods in Engineering. 1996;39:3839-66.
[7] Onate E, Idelsohn SR, Del Pin F, Aubry R. The particle finite element method, an overview. International Journal for Computational Methods. 2004;1:267-307.
[8] Lucy LB. A numerical approach to the testing of the fission hypothesis. Astron. 1977;J. 82 1013–24.
[9] Gingold RA, Monaghan JJ. Smoothed particle hydrodynamics: theory and application to non-spherical stars. Mon Not R Astron Soc. 1977 181 375–89.
[10] Dong XW, Liu GR, Li Z, Zeng W. A smoothed particle hydrodynamics (SPH) model for simulating surface erosion by impacts of foreign particles. Tribology International. 2016;95:267-78.
[11] Ngo-Cong D, Tran CD, Mai-Duy N, Tran-Cong T. Incompressible smoothed particle hydrodynamics-moving IRBFN method for viscous flow problems. Engineering Analysis with Boundary Elements. 2015;59:172-86.
[12] Saunders K, Prakash M, Cleary PW, Cordell M. Application of Smoothed Particle Hydrodynamics for modelling gated spillway flows. Applied Mathematical Modelling. 2014;38:4308-22.
[13] Tartakovsky AM, Panchenko A. Pairwise Force Smoothed Particle Hydrodynamics model for multiphase flow: Surface tension and contact line dynamics. Journal of Computational Physics. 2016;305:1119-46.
[14] Tofighi N, Ozbulut M, Rahmat A, Feng JJ, Yildiz M. An incompressible smoothed particle hydrodynamics method for the motion of rigid bodies in fluids. Journal of Computational Physics. 2015;297:207-20.
[15] Price D. Smoothed Particle Hydrodynamics and Magnetohydrodynamics. 2004.
[16] Cleary PW. Extension of SPH to predict feeding, freezing and defect creation in low pressure die casting. Applied Mathematical Modelling. 2010;34:3189-201.
[17] Cleary PW, Ha J, Prakash M, Nguyen T. 3D SPH flow predictions and validation for high pressure die casting of automotive components. Applied Mathematical Modelling. 2006;30:1406-27.
[18] Pineau F, D'Amours, G. Applicaiton of LS-DYNA SPH formulation to model semi-solid metal casting - Skin layers. 8th European LS-DYNA Users Conference. 2011.
[19] Cleary PW, Prakash M, Das R, Ha J. Modelling of metal forging using SPH. Applied Mathematical Modelling. 2012;36:3836-55.
[20] Tanaka K. Numerical studies on the explosive welding by smoothed particle hydrodynamics (sph).
[21] Fraser K, St-Georges L, Kiss LI, Chiricota Y. Hybrid thermo-mechanical contact algorithm for 3D SPH-FEM multi-physics simulations. IV International Conference on Particle-Based Methods - Particles 2015. Barcelona, Spain2015.
[22] Limido J, Espinosa C, Salaün M, Lacome JL. SPH method applied to high speed cutting modelling. International Journal of Mechanical Sciences. 2007;49:898-908.
[23] Bhojwani S. Smoothed Particle Hydrodynamics modelling of the friction stir welding process. Ann Arbor, MI.: ProQuest; 2007.
[24] Timesli A, Zahrouni H, Braikat B, Moufki A, Lahman H. Numerical model based on SPH to simulate friction stir welding. Revue de mechanique appliquee et theorique. 2011;2:537-46.
[25] Tartakovsky AM, Grant G, Sun X, Khaleel M. Modeling of friction stir welding process with smooth particle hydrodynamics. SAE International. 2006.
[26] Pan W, Li D, Tartakovsky AM, Ahzi S, Khraisheh M, Khaleel M. A new smoothed particle hydrodynamics non-Newtonian model for friction stir welding: Process modeling and simulation of microstructure evolution in a magnesium alloy. International Journal of Plasticity. 2013.
[27] Fraser K, St-Georges L, Kiss LI. Prediction of defects in a friction stir welded joint using the Smoothed Particle Hydrodynamics Method. Procedings of the 7th Asia Pacific IIW International Congress on Recent Development in Welding and Joining Methods. Singapore2013.
[28] Fraser K, St-Georges L, Kiss LI. Smoothed Particle Hydrodynamics Numerical Simulation of Bobbin Tool Friction Stir Welding. 10th International Friction Stir Welding Symposium. Beijing China: TWI; 2014.
[29] Bonet J, Kulasegaram S. A simplified approach to enhance the performance of smooth particle hydrodynamics methods. Applied Mathematics and Computation. 2002;126:133-55.
[30] Hoover WG. Smooth Particle Applied Mechanics: The State of the Art (Advanced Series in Nonlinear Dynamics). Singapore: World Scientific Publishing; 2006.

[31] Liu GR, Liu MB. Smoothed particle hydrodynamics : a meshfree particle method. Hackensack, New Jersey: World Scientific; 2003.
[32] Monaghan JJ. Smoothed Particle Hydrodynamics - A Review 1977 to 2005. Rep Prog Phys. 2005;68 1703.
[33] Violeau D. Fluid Mechanics and the SPH Method. United Kingdom: Oxford University Press; 2014.
[34] Cleary PW, Monaghan JJ. Conduction Modelling Using Smoothed Particle Hydrodynamics. Journal of Computational Physics. 1998.
[35] Rook R, Yildiz M, Dost S. Modeling Transient Heat Transfer Using SPH and Implicit Time Integration. Numerical Heat Transfer, Part B: Fundamentals. 2007;51:1-23.
[36] Marrone S, Colagrossi A, Le Touzé D, Graziani G. Fast free-surface detection and level-set function definition in SPH solvers. Journal of Computational Physics. 2010;229:3652-63.
[37] Randles PW, Libersky LD. Smoothed Particle Hydrodynamics: Some recent improvements and applications. Computer Methods in Applied Mechanics and Engineering. 1996;139:375-408.
[38] Fraser K. Adaptive smoothed particle hydrodynamics neighbor search algorithm for large plastic deformation computational solid mechanics. 13th International LS-DYNA Users Conference. Dearborn Michigan: LSTC; 2014.